Crystalline−Crystalline Diblock Copolymers of Linear Polyethylene and Hydrogenated Polynorbornene

Sasha B. Myers and Richard A. Register*

Department of Chemical Engineering, Princeton University, Princeton, New Jersey 08544-5263

Received April 4, 2008; Revised Manuscript Received July 1, 2008

ABSTRACT: Double-crystalline diblock copolymers of linear polyethylene (LPE) and hydrogenated polynorbornene (hPN) are synthesized, and their crystallization is examined. LPE and hPN homopolymers are both highly crystalline, with similar melting points near 150 °C and $\chi_{hPN/LPE} = 0.02$. For symmetric diblocks, even when moderately segregated, crystallization of hPN breaks out of the melt microdomains to create volume-filling spherulites. The LPE block subsequently crystallizes between the hPN crystallites, with the hPN and LPE crystal stems oriented orthogonally. At shallow undercoolings, crystallization proceeds in two distinct steps, but at deeper undercoolings, only a single process is observed, following the temperature dependence of hPN crystallization. At these deeper undercoolings, crystallization of hPN initiates LPE crystallization so that the two processes are nearly simultaneous. By changing the block ratio, the crystallization behavior can be broadly tuned: in hPN-rich diblocks, the two crystallization processes are well-separated at any temperature, while in LPE-rich diblocks, the LPE block crystallizes first.

Introduction

Semicrystalline block copolymers have been a subject of strong interest during the past 15 years.[1−3] Typically, semicrystalline diblock copolymers contain one crystallizable and one amorphous block. These blocks may be mixed or microphase-separated in the melt, and if phase-separated, the amorphous block may be either above or below its glass transition at the freezing point of the crystallizable block, all with substantial consequences for the solid-state structure and the crystallization kinetics.[1−4] Block copolymers containing two chemically distinct crystallizable blocks have been the subject of fewer studies, as summarized in a recent review.[4] These materials potentially offer an even richer array of behaviors, since the solid-state structure can be set by the microphase-separated melt or by crystallization of either block. In any case, at least one of the blocks—the one which is second to crystallize—must crystallize under confined conditions, where the confining structure is set either by the microphase-separated melt or through the lamellar crystalline structure established by crystallization of the first block. Moreover, it may be possible to access these various crystallization scenarios within a single block copolymer system by changing the block molecular weights or even by changing the crystallization history.

In general, the melting points of the two homopolymers which one might combine into a block copolymer are quite different, so that there is little question as to which component will be the first to crystallize. Accessing the full range of behaviors within a single system requires that blocks with generally similar melting points be chosen. The best studied example[5−9] in this regard is poly(ε-caprolactone)−poly(ethylene oxide), PCL/PEO, which was first examined by Perret and Skoulios.[5,6] For a near-symmetric PCL/PEO/PCL triblock copolymer (total M_n = 17 000 g/mol), they observed clear two-step crystallization behavior by dilatometry, corresponding to sequential crystallization of the PCL and PEO blocks; moreover, which block crystallized first could be changed simply through the crystallization temperature. However, the synthesis of PCL/PEO diblock and triblock copolymers is usually limited to low molecular weights (<20 000 g/mol), with the polydispersity increasing markedly for higher molecular weights.[7−9] In addition, the relatively low melting points of PEO and PCL, ca. 65 °C, limit their utility.

Here, we describe the synthesis, structural characterization, and crystallization behavior of novel diblock copolymers combining two highly crystalline saturated hydrocarbon polymers: linear polyethylene (LPE), also known as high-density polyethylene, and hydrogenated polynorbornene (hPN). LPE[10] and hPN[11] homopolymers are both highly crystalline (typically >70%), with no chain defects to limit the crystal thickness; in this respect, both differ significantly from the low-crystallinity poly(ethylene-*co*-butene), or hydrogenated polybutadiene, which has been widely employed as a component of model crystallizable block copolymers.[1,2,12] LPE and hPN also have similar and usefully high equilibrium melting points: $T_{m,LPE}^\circ$ = 145.8 °C[13] and $T_{m,hPN}^\circ$ = 156 °C.[11] Our hPN/LPE diblocks are synthesized by sequential living ring-opening metathesis polymerization (ROMP) of norbornene and cyclopentene, followed by catalytic hydrogenation. The living nature of the polymerization permits the targeted synthesis of well-defined diblock copolymers of broadly tunable molecular weight and composition, while the thermal stability of the fully saturated products permits their behavior to be examined over a wide range of temperatures.

Experimental Section

Synthesis. hPN/LPE diblock copolymers were synthesized by ring-opening metathesis polymerization (ROMP), followed by hydrogenation. The norbornene block was polymerized first, as norbornene polymerizes to essential completion, while cyclopentene does not.[10] All ROMP reactions were run under a nitrogen atmosphere in an Innovative Technologies glovebox (~0.7 ppm of O_2, ~0.5 ppm of H_2O), with the Schrock-type initiator 2,6-diisopropylphenylimidoneophylidenemolybdenum(VI) bis(*tert*-butoxide) (Strem Chemicals, used as received). Norbornene (99%, Aldrich Chemical) and polymerization regulator trimethylphosphine (PMe_3) were each dried over freshly cut sodium, degassed by freeze−pump−thaw cycles, and vacuum transferred prior to use. Cyclopentene monomer (96%, Aldrich) and toluene were each dried over diphenylhexyllithium (adduct of butyllithium and diphenylethylene), degassed by freeze−pump−thaw cycles, and vacuum transferred. The Mo initiator was added to toluene (at a concentration determined by the desired molecular weight[10] of the second block, PCP), followed by the addition of a concentrated norbornene

* Corresponding author. E-mail: register@princeton.edu.

10.1021/ma800759b CCC: $40.75 © 2008 American Chemical Society
Published on Web 08/19/2008

Table 1. Characteristics of Block Copolymers and Homopolymers

sample code (hPN/LPE)	hPN block M_n (g/mol)	hPN block M_w/M_n	LPE M_n (g/mol)	diblock M_w/M_n	volume fraction hPN at 160 °C (f_{hPN})
42/55	41 900	1.10	54 700	1.10	0.40
26/26	26 300	1.07	25 800	1.11	0.47
37/13	37 200	1.17	12 900	1.16	0.72
10/42	10 000	1.13	41 500	1.17	0.18
hPN	60 000	1.11			1
LPE			20 000	1.07[a]	0

[a] Polydispersity of the LPE homopolymer.

solution in toluene, and stirred for 60 min to ensure complete polymerization of the norbornene.[14] The concentration of norbornene in toluene was varied from 1 to 8 wt %, according to the desired PN/PCP ratio in the final diblock. PMe_3 was then added (5 equiv vs Mo), followed by cyclopentene to a concentration of 3 M. The reaction mixture was stirred for 60 min and terminated with butyraldehyde (>10 equiv vs Mo; Aldrich, Sure/Seal, used as received). The mixture was stirred for an additional 30 min; the polymer was recovered and purified by repeated precipitation into methanol and dried under vacuum at room temperature.

Hydrogenation of the PN/PCP diblocks to hPN/LPE was carried out in a stirred Parr reactor, in cyclohexane at 0.5 wt % polymer, over palladium catalyst supported on calcium carbonate ($Pd^0/CaCO_3$, Pd^0 content 5 wt %, Alfa Aesar; approximately 1:20 ratio of Pd^0 to polymer).[10] A minimum of 400 psig hydrogen was employed at 100 °C. Hydrogenation was continued for 1−3 days until the *trans* C=C double bond stretch at 966 cm^{-1} in the infrared spectrum was reduced to baseline, which corresponds to >99.95% saturation.

Molecular Characterization. Characterization was conducted on the soluble, unsaturated PN/PCP diblocks, as previous work has shown that under these conditions hydrogenation of PN[15] and PCP[10] does not lead to any backbone rearrangements. Gel permeation chromatography (GPC) in tetrahydrofuran (THF) was used to determine polymer molecular weights and polydispersities, using a Waters 515 HPLC pump, two 30 cm Polymer Laboratories PLgel Mixed-C columns, and a Waters 410 differential refractometer detector. The GPC system was calibrated with narrow-distribution polystyrene standards, and the results converted to true molecular weights via division by the hydrodynamic correction factor $R = 1.78$ for PN in THF.[14] PN block molecular weights and polydispersities were determined by measurement of a small sample of the first block taken from the reaction just prior to charging the CP monomer. Diblock polydispersities were measured by GPC on the products, which showed undetectable levels of terminated first block (PN). Block copolymer compositions were determined by ^1H NMR, using the olefinic protons from both repeat units and the methine protons from the PN block. PCP block molecular weights were determined from the diblock compositions and the PN block molecular weights. To complement the diblocks, measurements were also made on hPN[11] and LPE[10] homopolymers synthesized analogously and characterized previously. Polymer characteristics are given in Table 1, after correction for the small mass uptake (2 g/mol per repeat unit) due to hydrogenation. Volume fractions of hPN in the melt at 160 °C, f_{hPN}, were calculated with mass densities of 0.879 g/cm^3 for hPN[16] and 0.771 g/cm^3 for LPE.[17] Diblocks will be referred to by their hPN/LPE block molecular weights (in kg/mol).

Thermal and Morphological Characterization. Differential scanning calorimetry (DSC) measurements on ca. 10 mg specimens employed a Perkin-Elmer DSC 7 equipped with an intracooler and calibrated with indium and mercury. In addition to scanning measurements at 10 °C/min, isothermal crystallizations were also conducted with this system.

Wide- and small-angle X-ray scattering (SAXS and WAXS) employed two systems run from a common PANalytical PW3830 generator with long fine focus Cu X-ray tube to yield Cu Kα radiation. All data were collected in transmission, and each system was equipped with its own hot stage. WAXS measurements employed a Statton pinhole camera system previously described,[18] using Kodak image plates read by a GE Biosciences Storm 820 scanner. The isotropic two-dimensional patterns were converted to one-dimensional traces of intensity vs scattering angle 2θ, calibrated[11] with NaCl. SAXS measurements employed an Anton-Paar compact Kratky camera and MBraun OED-50 M position-sensitive detector. Data were corrected for detector sensitivity and positional linearity, empty beam scattering, and sample thickness and transmittance, placed on an absolute intensity scale via a polyethylene standard, and desmeared for slit length.[19] Intensities are presented against the magnitude of the momentum transfer vector $q = (4\pi/\lambda) \sin\theta$, where θ is half the scattering angle; calibration was via a silver behenate[20] standard ($d = 5.838$ nm).

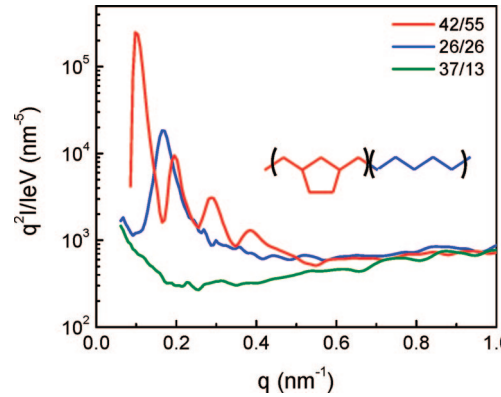

Figure 1. SAXS patterns for three hPN/LPE diblocks in the melt at 160 °C. hPN/LPE 42/55 and 26/26 show ordered melts, while hPN/LPE 37/13 is disordered. The repeat unit structure of hPN (red)/LPE (blue) is shown in the inset, with the LPE repeat based on the repeat unit of its PCP precursor.

Results and Discussion

Melt Morphology. Figure 1 shows small-angle X-ray scattering (SAXS) patterns for three representative hPN−LPE diblocks in the melt at 160 °C. The highest molecular weight diblock, hPN/LPE 42/55 ($f_{hPN} = 0.40$), clearly forms a lamellar melt, with peaks observed in a q ratio of 1:2:3:4. hPN/LPE 26/26, also near-symmetric ($f_{hPN} = 0.47$) but of lower molecular weight, shows only a single sharp reflection. This indicates an ordered melt, and we infer from the composition that its morphology is also lamellar. By contrast, the pattern for the asymmetric hPN/LPE 37/13 ($f_{hPN} = 0.72$) is featureless, indicating a disordered melt. These observations, combined with the self-consistent-field phase diagram applicable for long-chain block copolymers,[21] allow us to bracket the interaction energy density between LPE and hPN as $X = 0.75 \pm 0.15$ J/cm^3 at 160 °C; with a representative reference segment of 83 g/mol (average of hydrogenated norbornene and hydrogenated cyclopentene, five backbone carbons each, as shown in the inset to Figure 1), this translates to a Flory interaction parameter $\chi = 0.020 \pm 0.004$ at 160 °C. This is a typical interaction energy density for blends of saturated hydrocarbon polymers: smaller than that between LPE and polypropylene,[22] or between LPE and polyvinylcyclohexane (PVCH),[23] and comparable to that between LPE and an ethylene copolymer containing 70 wt % α-olefin.[24]

Though both hPN/LPE 42/55 and 26/26 possess ordered melts, the segregation strength—at most double that at the order−disorder transition, for 42/55—is insufficient to prevent crystals from "breaking out" of the melt structure.[25,26] All of our hPN/LPE polymers show volume-filling, negatively birefringent spherulites when examined by polarizing optical microscopy, regardless of whether the melt was ordered or disordered. Furthermore, wide-angle X-ray scattering (presented

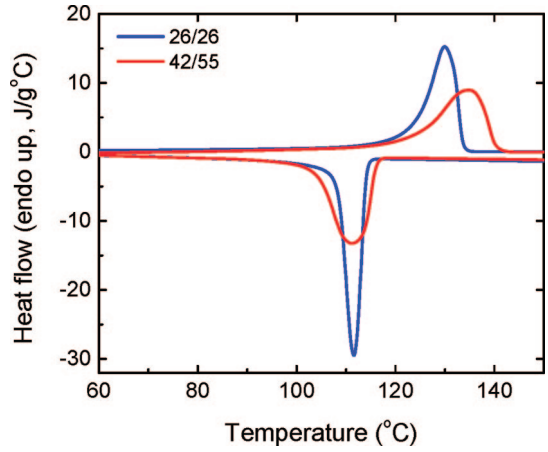

Figure 2. DSC heating and cooling thermograms (10 °C/min) for hPN/LPE 26/26 (blue) and hPN/LPE 42/55 (red). Only a single endo/exothermic process is observed for each polymer.

below) demonstrates that both blocks are crystalline at room temperature. Yet DSC heating/cooling scans of hPN/LPE 42/55 and 26/26, shown in Figure 2, reveal only a single endo/exothermic process, suggesting that the hPN and LPE blocks have similar melting temperatures and that they crystallize nearly simultaneously as well.

To reveal the sequence of crystallization and melting in these diblocks, we employed hot-stage WAXS. Figure 3a presents WAXS patterns for hPN/LPE 26/26 collected during stepwise heating. At these high temperatures, hPN crystals are in the rotationally disordered pseudohexagonal phase;[11] the observed peak corresponds to the (100) reflection of a hexagonal lattice with $a_{hex} = 0.552$ nm. For LPE, the (110) and (200) peaks for the usual orthorhombic unit cell[17] are visible. Though the melting ranges of the two blocks overlap, it is clear from the progressive diminution of the LPE peaks upon heating that LPE melts first. Similarly, Figure 3b shows time-resolved WAXS measurements during an isothermal hold at 122 °C following a quench from the 160 °C melt. After 30 min, nearly all the observed crystallinity is from hPN, but after 60 min both blocks have crystallized substantially. WAXS measurements on hPN/LPE 42/55 are qualitatively similar.[27] For both diblocks, hPN crystallizes first and sets up the spherulitic superstructure; the LPE block must then crystallize within the spaces between hPN crystals. Thus, these diblocks are examples of both unconfined crystallization (of the hPN block) and confined crystallization (of the LPE block).

None of these observations provides any insight into the arrangement of the hPN and LPE crystals, however, for which we turned to hot-stage SAXS. Figure 4a shows the SAXS patterns for hPN/LPE 26/26 at 160 °C and after various times following a quench to 123 °C. In the first 15 min, we observe the clear coexistence of the ordered melt structure (with peak position $q^* = 0.16$ nm^{-1}) with a second structure, evidently the semicrystalline solid, with a much larger Bragg spacing ($q^* = 0.095$ nm^{-1}). In the next two time increments (30 and 45 min), the peak for the semicrystalline solid increases in intensity, while that for the ordered melt decreases and disappears. Thus, crystallization of hPN (and conversion of the ordered melt to the semicrystalline solid) is essentially complete after 45 min. However, at times beyond 45 min, the primary peak near 0.095 nm^{-1} *diminishes* in intensity, by a factor of 2, while the intensity near $q = 0.19$ nm^{-1} *increases* strongly. These changes reflect the crystallization of LPE: the primary peak diminishes in intensity because the electron density contrast is reduced upon LPE crystallization. At 123 °C, the relevant electron densities are calculated to be LPE (amorphous)[17] = 272 e$^-$/nm^3, LPE (crystalline)[17] = 334 e$^-$/nm^3, hPN (amorphous)[16] = 304 e$^-$/nm^3, and hPN (crystalline)[16] = 329 e$^-$/nm^3. Simultaneously, the primary peak shifts slightly but systematically to higher q (from 0.095 nm^{-1} at 45 min, progressively to 0.099 nm^{-1} at 120 min). This 4% reduction in Bragg spacing reflects the density change on going from amorphous to semicrystalline LPE layers.

Hamley et al.[28] studied a different double-crystalline diblock—poly(L-lactic acid)/poly(L-caprolactone), PLLA/PCL, wherein PLLA crystallizes first—and observed similar changes in SAXS pattern upon PCL crystallization during dynamic cooling: the primary peak scarcely moved or broadened but decreased severalfold in intensity, while the intensity at higher q (near the initial second-order peak) increased. This was briefly described as "pointing to a significant variation in the lamellar crystal stacking", but the data in Figure 4a can provide deeper insight into the arrangement of hPN and LPE crystallites in the solid state: they indicate that when LPE crystallizes, it stacks orthogonally to the structure established by hPN, as indicated in the schematic in Figure 4b. In this case, the electron density of the LPE domain in the hPN stacking direction (along d_{hPN} in the schematic) is a simple lateral average of the crystalline and amorphous LPE densities. By contrast, if the LPE lamellae were to grow parallel to the hPN lamellae (LPE crystal stems along d_{hPN} direction), this would effectively halve the periodicity of the primary structure and eradicate the peak near 0.099 nm^{-1}, as the electron densities for crystalline hPN and LPE are quite similar. The increased intensity near $q = 0.19$ nm^{-1}, which develops between 45 and 120 min, reflects the additional scattering from stacks of LPE crystals which form orthogonally to the hPN crystals, with a periodicity d_{LPE} roughly half d_{hPN}. This type of structure, where the LPE crystal stems are oriented parallel to the pre-existing lamellar interface, is quite similar to that already established for crystallization of poly(ethylene-*co*-butene) confined either by glassy PVCH lamellae[29,30] or in segregated melts where the microdomain structure is retained.[29−31] In their early study of a low-molecular-weight, near-symmetric PCL/PEO/PCL triblock copolymer, Perret and Skoulios[6] also observed a puzzling two sets of Bragg reflections for a narrow range of crystallization temperatures (49−51 °C), where PEO crystallizes first. Those results may be interpreted analogously, assigning the larger spacing to the PEO crystals and the smaller spacing to the PCL crystals.

Confinement of the LPE block between hPN lamellae might be expected to strongly impact its crystallization kinetics, similar to the case where the confinement is between glassy lamellae.[32] Moreover, the WAXS and SAXS data in Figures 3 and 4 suggest that at shallow undercoolings hPN and LPE crystallize at sufficiently different rates to probe them independently, despite the extensive overlap of these processes during DSC heating/cooling at 10 °C/min (Figure 2). Figure 5 shows the results of DSC isothermal crystallizations for hPN/LPE 42/55 and 26/26 at various undercoolings, presented as integrated enthalpies (remaining fraction of total heat release vs time). At shallow undercoolings, the integrated heat release curve develops an inflection point, and for hPN/LPE 26/26, the curve clearly splits into two steps for the shallowest undercoolings. (For hPN/LPE at the shallowest undercoolings, the second step is incomplete even at long times, so the fractional enthalpy release was normalized to the average total enthalpy measured at lower crystallization temperatures.) The 1:3 enthalpy ratio for the first: second process is as expected for a near-symmetric diblock, since the heats of fusion of 100% crystalline hPN (86 J/g)[15] and LPE (277 J/g)[17] are in a similar ratio.

The LPE crystallization process, which occurs second at shallow undercoolings, clearly has a much stronger dependence on temperature than does hPN crystallization, as is true for the

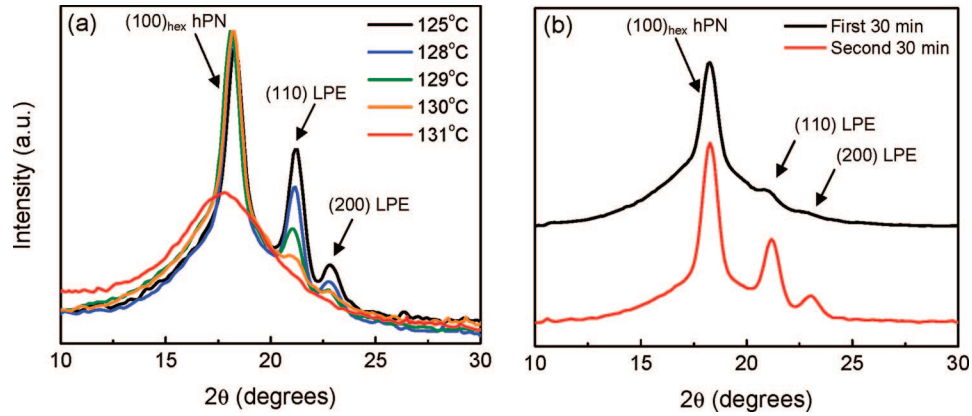

Figure 3. (a) WAXS patterns of hPN/LPE 26/26 during heating, following a quench from 160 °C to room temperature. Peaks are labeled with Miller indices for the relevant planes in LPE and hPN. LPE melting precedes hPN melting. (b) WAXS patterns for hPN/LPE 26/26 taken during isothermal crystallization at 122 °C, after quenching from the melt at 160 °C. Top curve (black) represents the intensity integrated over the first 30 min at 122 °C, while the bottom curve (red) was collected over the next 30 min (30−60 min after reaching 122 °C). hPN crystallization precedes LPE crystallization. Curves are normalized to equal area and offset in intensity for clarity.

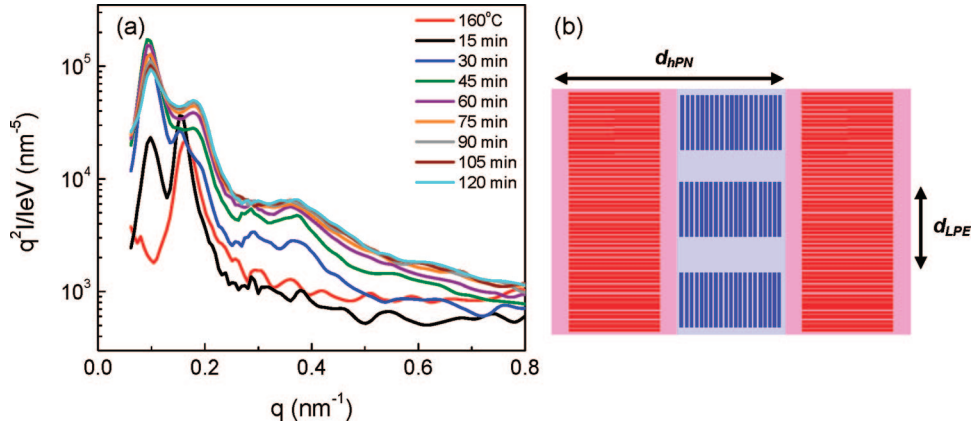

Figure 4. (a) SAXS patterns for hPN/LPE 26/26 at 123 °C after cooling from the melt (160 °C, red curve). Each pattern was captured over the 15 min prior to its time stamp. (b) Schematic illustrating solid-state domain structure in hPN/LPE diblocks. Dark lines represent crystal stems, with amorphous regions indicated by paler shades. hPN (red) crystallizes first to set up a lamellar structure with periodicity d_{hPN} (= 63 nm for data shown in panel a). LPE (blue) subsequently crystallizes between hPN lamellae, stacking orthogonally to the hPN, with a periodicity d_{LPE} (≈33 nm for data shown in panel a).

LPE and hPN homopolymers (Figure 5c). Therefore, we hypothesized that at deep undercoolings the processes might reverse: that DSC would again show a two-step process, but with LPE crystallizing first. However, the integrated heat release curves in Figure 5a,b do not show such behavior. As the undercooling is increased, the two processes merge into one but do not split again even at the deepest undercoolings at which isothermal crystallizations could be conducted. These curves are adequately described by the Avrami equation[32] with exponent $n = 2.3 \pm 0.3$, with no clear dependence on undercooling. In addition, the crystallization half-times $t_{1/2}$, where half of the total heat release has occurred, show the same temperature dependence (slope of log $t_{1/2}$ vs T curve) as the hPN homopolymer, as shown in Figure 5c. This suggests that even at the deeper undercoolings hPN crystallizes first but that crystallization of hPN then "triggers" the crystallization of the LPE chains confined between hPN crystals. Müller and co-workers[34−36] observed a related phenomenon for poly(*p*-dioxanone)/poly(ε-caprolactone) diblocks, PPDX/PCL, where the crystallization of PCL in PCL-rich diblocks (≥60 wt % PCL) was accelerated—relative to PCL homopolymer—by prior crystallization of the PPDX block, referred to as a "nucleating effect" of PPDX on PCL.

Why the LPE crystallization rate is enhanced upon hPN crystallization is not certain. There is no obvious epitaxial relationship between the hPN and LPE crystals, and in any case, the fold surfaces of the hPN crystals (schematic in Figure 4b) are expected to be amorphous. But we note the 70% increase in domain spacing which occurs upon hPN crystallization for hPN/LPE 26/26 (Figure 4a). Even in the melt, block copolymer chains are already stretched away from the interface (ideally as $M^{2/3}$, in the strong segregation limit[21]); when q^* increases by 70%, so does the thickness of the molten LPE layer, with a concomitant increase in chain stretching. This additional chain orientation in the melt may then accelerate LPE crystallization.

hPN-Rich Diblock. To better separate the two crystallization processes, we investigated the crystallization behavior of hPN/LPE 37/13, which has a molecular weight similar to hPN/LPE 26/26 but an hPN-rich composition. As already discussed (Figure 1), hPN/LPE 37/13 forms a homogeneous melt. By lengthening the hPN block (vs hPN/LPE 26/26), we expect to raise its T_m and T_c, while shortening the LPE block should concomitantly lower its T_m and T_c. Figure 6a shows that this difference in relative block length does indeed split the single endo/exotherm observed by DSC for hPN/LPE 26/26 (Figure 2) into two for hPN/LPE 37/13. Hot-stage WAXS experiments[27] analogous to those in Figure 3 confirm that the hPN block is the last to melt and the first to crystallize. Though the mass ratio of hPN:LPE is approximately 3:1 in hPN/LPE 37/13, the areas of the two DSC peaks are comparable due to the ∼1:3 ratio of the heats of fusion for hPN:LPE. From the peak melting

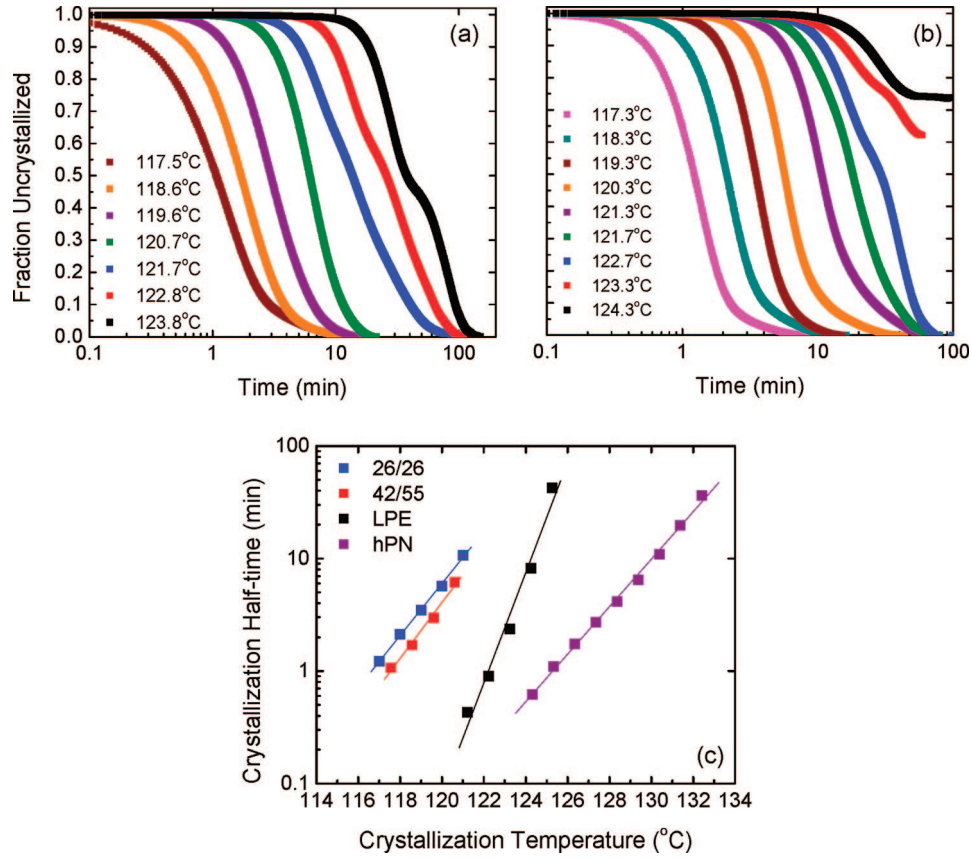

Figure 5. Isothermal crystallization kinetics for (a) hPN/LPE 42/55 and (b) hPN/LPE 26/26 at the temperatures indicated in the keys. The process is adequately described by the Avrami equation up to ~121 °C for hPN/LPE 42/55 and to ~121.5 °C for hPN/LPE 26/26, where the curve develops an inflection point and then splits into two steps. (c) Crystallization half-time (50% of total enthalpy released) as a function of the crystallization temperature for hPN/LPE 26/26 and 42/55 as well as LPE and hPN homopolymers. For the diblocks, only data for the single-step process (temperatures below that where the inflection point develops) are included.

temperatures of 135.5 °C (hPN) and 122.6 °C (LPE), we may estimate the hPN and LPE crystal thicknesses t from the Gibbs−Thomson equation written for platelike crystals,[33] with the known equilibrium melting points, heats of fusion, crystal densities ($\rho_{xtal,hPN}$[11] = 0.970 g/cm^3, $\rho_{xtal,LPE}$[17] = 0.973 g/cm^3), and fold surface energies (σ_{hPN}[15] = 0.045 J/m^2, σ_{LPE}[13] = 0.089 J/m^2). The results are t_{hPN} = 23 nm and t_{LPE} = 12 nm, consistent with the schematic in Figure 4b, where the confined LPE crystals are thinner than the unconfined hPN crystals.

The isothermal crystallization rates of the two blocks in hPN/LPE 37/13 are quite distinct as well. hPN crystallization is easily completed prior to the development of substantial LPE crystallinity. Figure 6b shows DSC results for isothermal crystallizations of the hPN block alone, at several different temperatures. Again, these sigmoidal curves are adequately described by the Avrami equation, with exponents $n = 3.2 \pm 0.8$. For measurement of LPE crystallization, the specimen was first quenched from the melt to 120 °C and held for 15 min to fully crystallize the hPN block. The specimen was then stepped to a lower temperature and held isothermally to crystallize the LPE block. This second crystallization step, shown in Figure 6c on a linear time scale, is adequately described by a simple exponential decay, i.e., an Avrami exponent $n = 1$. Such first-order kinetics are observed when polymers are confined within tiny isolated regions, such as block copolymer microdomains; in that case, each domain must be independently and homogeneously nucleated, and crystal growth to the full extent of the domain is essentially instantaneous once nucleation has occurred.[32,37,38] However, the temperatures represented in Figure 6c are too high for substantial homogeneous nucleation to be occurring; at 116 °C, the homogeneous nucleation rate of LPE is estimated[39,40] at only 10^{-25} nuclei/(μm^3 min). Thus, while the small value of the Avrami exponent (vs n = 2.8 for LPE homopolymer[27]) indicates that the pre-existing hPN framework strongly perturbs the crystallization of LPE, we do not infer that the LPE is divided into isolated pockets which must be individually nucleated. Rather, it appears that LPE crystallization is nucleated heterogeneously, possibly by the same extrinsic nuclei responsible for hPN crystallization. Interestingly, the temperature dependences of the two steps (slope of log $t_{1/2}$ vs T curves in Figure 6d) are essentially the same as those of the two homopolymers, implying that the processes are largely independent, despite the fact that the hPN and LPE crystallites are intimately intermixed.

LPE-Rich Diblock. For each of the three diblocks described in the preceding sections, hPN crystallizes first, begging the question of whether the LPE can ever be the templating block in the hPN/LPE system. Toward this end, we synthesized a diblock, hPN/LPE 10/42, again having a molecular weight near 50 kg/mol but with a 4:1 LPE:hPN mass ratio. As with the hPN-rich diblock (hPN/LPE 37/13), hPN/LPE 10/42 also shows a single-phase melt by SAXS[27] at 160 °C. For this polymer, DSC is of little utility; given the block ratio and the heats of fusion of the homopolymers, the total enthalpy of crystallization is heavily dominated (>90%) by crystallization of the LPE, making the crystallization of hPN difficult to detect. However, hot-stage WAXS still provides important information, as shown in Figure 7. Following a quench to 128 °C from the 160 °C melt, crystallization of the LPE is observed and is essentially complete after 90 min. During this same period, no visible crystallization of hPN occurs (no sharp peak at 2θ = 18.6°).

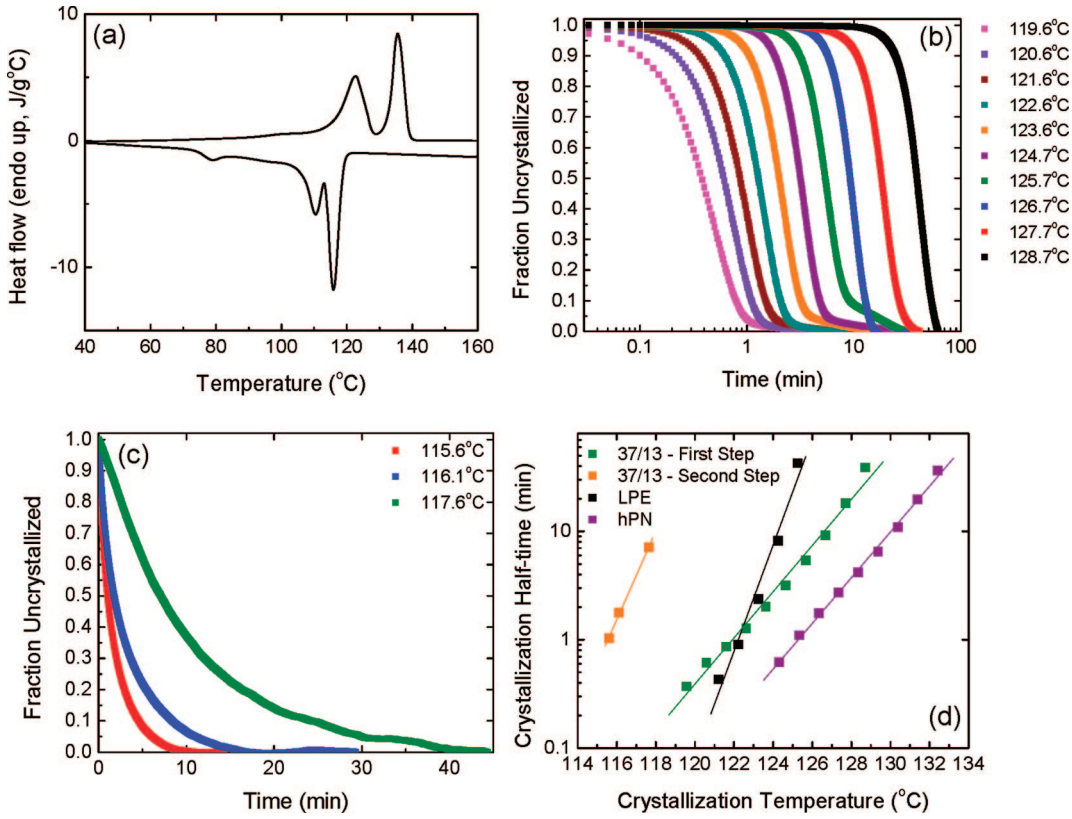

Figure 6. (a) DSC heating and cooling thermograms (10 °C/min) for hPN/LPE 37/13. The lower temperature peak in each trace corresponds to LPE and the higher temperature peak to hPN. (b) Heat release curves during isothermal crystallizations of hPN/LPE 37/13 at shallow undercoolings, where only the hPN block crystallizes. (c) Heat release curves during isothermal crystallizations of hPN/LPE at deeper undercoolings, subsequent to complete hPN crystallization; only LPE participates. Note change to linear time axis. (d) Crystallization half-times for hPN/LPE 37/13, extracted from data in panels b and c, along with half-times for hPN and LPE homopolymers.

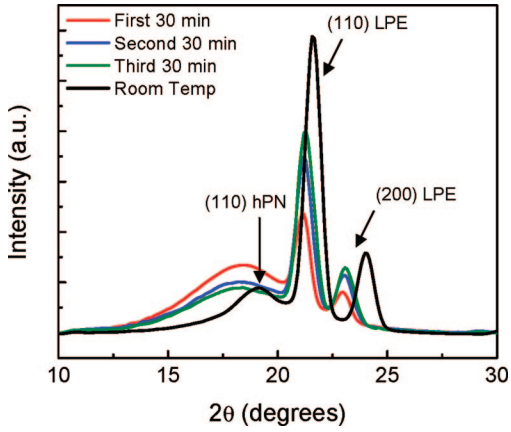

Figure 7. WAXS patterns for hPN/LPE 10/42 taken during isothermal crystallization at 128 °C, after quenching from the 160 °C melt. Patterns were captured over successive 30 min intervals. At 128 °C, only LPE crystallizes within the first 90 min. The final pattern (black) was taken after cooling to room temperature, where hPN has also crystallized.

Upon further cooling to room temperature, the (110) and (200) LPE peaks shift due to the temperature dependence of the unit cell dimensions,[17] and concurrently the broad hump present in the melt at $2\theta = 18.5°$ is replaced by a relatively narrow peak at $2\theta = 19.1°$. At room temperature, hPN homopolymer shows a monoclinic structure with the most intense peak, the (110), at 19.1°, confirming that hPN does crystallize within the LPE framework upon cooling from 128 °C to room temperature.

Conclusions

hPN/LPE diblock copolymers represent a versatile system for the study of crystalline−crystalline block copolymers, as living ROMP permits the synthesis of such polymers with well-defined block architectures, low polydispersities, and a broad range of compositions and molecular weights. The similar melting points of hPN and LPE allow the identity of the first-crystallizing block (hPN or LPE) to be manipulated through the relative block lengths in the copolymers. In near-symmetric polymers, even those with microphase-separated melts (with χN double that at the order−disorder transition), crystallization of the hPN blocks sets the structural framework, forcing the LPE block to crystallize between the hPN lamellae. Analysis of the SAXS patterns during isothermal crystallization indicates that the LPE crystals stack with their normals parallel to the hPN−LPE domain interfaces, analogous to crystallization confined by glassy lamellae. At shallow undercoolings, two-step crystallization kinetics are observed (hPN followed by LPE), but at deeper undercoolings, only a single process is observed, with a temperature dependence that parallels that for the hPN homopolymer. At these deeper undercoolings, crystallization of the hPN block triggers crystallization of the LPE block.

Acknowledgment. This work was supported by the National Science Foundation, through the Polymers Program (DMR-0505940) and through a Graduate Research Fellowship to S.B.M.

References and Notes

(1) Hamley, I. W. *Adv. Polym. Sci.* **1999**, *148*, 113–137.
(2) Loo, Y.-L.; Register, R. A. In *Developments in Block Copolymer Science and Technology*; Hamley, I. W., Ed.; John Wiley & Sons Ltd.: Chichester, 2004; p 213.
(3) Müller, A. J.; Balsamo, V.; Arnal, M. L. *Adv. Polym. Sci.* **2005**, *190*, 1–63.
(4) Müller, A. J.; Arnal, M. L.; Balsamo, V. *Lect. Notes Phys.* **2007**, *714*, 229–259.

(5) Perret, R.; Skoulios, A. *Makromol. Chem.* **1972**, *162*, 147–162.
(6) Perret, R.; Skoulios, A. *Makromol. Chem.* **1972**, *162*, 163–177.
(7) Takeshita, H.; Fukumoto, K.; Ohnishi, T.; Ohkubo, T.; Miya, M.; Takenaka, K.; Shiomi, T. *Polymer* **2006**, *47*, 8210–8218.
(8) He, C.; Sun, J.; Ma, J.; Chen, X.; Jing, X. *Biomacromolecules* **2006**, *7*, 3482–3489.
(9) Li, L.; Meng, F.; Zhong, Z.; Byelov, D.; de Jeu, W. H.; Feijen, J. *J. Chem. Phys.* **2007**, *126*, 024904.
(10) Trzaska, S. T.; Lee, L.-B. W.; Register, R. A. *Macromolecules* **2000**, *33*, 9215–9221.
(11) Lee, L.-B. W.; Register, R. A. *Macromolecules* **2005**, *38*, 1216–1222.
(12) Falk, J. C.; Schlott, R. J. *Macromolecules* **1971**, *4*, 152–154.
(13) Bair, H. E.; Huseby, T. W.; Salovey, R. *Polym. Prepr. (Am. Chem. Soc., Div. Polym. Chem.)* **1968**, *9*, 795–805.
(14) Hatjopoulos, J. D.; Register, R. A. *Macromolecules* **2005**, *38*, 10320–10322.
(15) Lee, L.-B. W.; Register, R. A. *Macromolecules* **2004**, *37*, 7278–7284.
(16) Lee, L.-B. W. Ph.D. Thesis, Princeton University, **2004**.
(17) Quirk, R. P.; Alsamarraie, M. A. A. In *Polymer Handbook*, 3rd ed.; Brandrup, J., Immergut, E. H., Eds.; Wiley: New York, 1989; p V/15.
(18) Dean, D. M.; Rebenfeld, L.; Register, R. A.; and Hsiao, B. S. *J. Mater. Sci.* **1998**, *33*, 4797–4812.
(19) Register, R. A.; Bell, T. R. *J. Polym. Sci., Part B: Polym. Phys.* **1992**, *30*, 569–575.
(20) Huang, T. C.; Toraya, H.; Blanton, T. N.; Wu, Y. *J. Appl. Crystallogr.* **1993**, *26*, 180–184.
(21) Matsen, M. W.; Bates, F. S. *Macromolecules* **1996**, *29*, 1091–1098.
(22) Krishnamoorti, R.; Graessley, W. W.; Dee, G. T.; Walsh, D. J.; Fetters, L. J.; Lohse, D. J. *Macromolecules* **1996**, *29*, 367–376.
(23) Adams, J. L.; Quiram, D. J.; Graessley, W. W.; Register, R. A.; Marchand, G. R. *Macromolecules* **1998**, *31*, 201–204.
(24) Reichart, G. C.; Graessley, W. W.; Register, R. A.; Lohse, D. J. *Macromolecules* **1998**, *31*, 7886–7894.
(25) Nojima, S.; Kato, K.; Yamamoto, S.; Ashida, T. *Macromolecules* **1992**, *25*, 2237–2242.
(26) Rangarajan, P.; Register, R. A.; Fetters, L. J.; Bras, W.; Naylor, S.; Ryan, A. J. *Macromolecules* **1995**, *28*, 4932–4938.
(27) Myers, S. B. Ph.D. Thesis, Princeton University, **2008**.
(28) Hamley, I. W.; Parras, P.; Castelletto, V.; Castillo, R. V.; Müller, A. J.; Pollet, E.; Dubois, P.; Martin, C. M. *Macromol. Chem. Phys.* **2006**, *207*, 941–953.
(29) Hamley, I. W.; Fairclough, J. P. A.; Ryan, A. J.; Bates, F. S.; Towns-Andrews, E. *Polymer* **1996**, *37*, 4425–4429.
(30) Hamley, I. W.; Fairclough, J. P. A.; Terrill, N. J.; Ryan, A. J.; Lipic, P. M.; Bates, F. S.; Towns-Andrews, E. *Macromolecules* **1996**, *29*, 8835–8843.
(31) Douzinas, K. C.; Cohen, R. E. *Macromolecules* **1992**, *25*, 5030–5035.
(32) Loo, Y.-L.; Register, R. A.; Ryan, A. J.; Dee, G. T. *Macromolecules* **2001**, *34*, 8968–8977.
(33) Strobl, G. *The Physics of Polymers*, 3rd ed.; Springer-Verlag: Berlin, 2007; pp 186−192.
(34) Albuerne, J.; Márquez, L.; Müller, A. J.; Raquez, J. M.; Degée, P.; Dubois, P.; Castelletto, V.; Hamley, I. W. *Macromolecules* **2003**, *36*, 1633–1644.
(35) Müller, A. J.; Albuerne, J.; Esteves, L. M.; Márquez, L.; Raquez, J. M.; Degée, P.; Dubois, P.; Collins, S.; Hamley, I. W. *Macromol. Symp.* **2004**, *215*, 369–382.
(36) Müller, A. J.; Albuerne, J.; Marquez, L.; Raquez, J. M.; Degée, P.; Dubois, P.; Hobbs, J.; Hamley, I. W. *Faraday Discuss.* **2005**, *128*, 231–252.
(37) Loo, Y.-L.; Register, R. A.; Ryan, A. J. *Phys. Rev. Lett.* **2000**, *84*, 4120–4123.
(38) Reiter, G.; Castelein, G.; Sommer, J.-U.; Röttele, A.; Thurn-Albrecht, T. *Phys. Rev. Lett.* **2001**, *87*, 226101.
(39) Koutsky, J. A.; Walton, A. G.; Baer, E. *J. Appl. Phys.* **1967**, *38*, 1832–1839.
(40) Loo, Y.-L. Ph.D. Thesis, Princeton University, **2001**.

MA800759B